Materials Physics and Mechanics. 2023;51(6): 54-64
Research article
http://dx.doi.org/10.18149/MPM.5162023_5

Submitted: May 17, 2023
Approved: July 14, 2023
Accepted: August 10, 2023

Effect of industrial hot rolling mode on microstructure and properties of low carbon bainitic steel

A.A. Zisman [1,2], S.N. Petrov [1,2], N.Yu. Zolotorevsky [2] ✉, E.A. Yakovleva [1]

[1] National research center "Kurchatov institute" - Central research institute of structural materials "Prometey", St. Petersburg, Russia

[2] Peter the Great St. Petersburg Polytechnic University, St. Petersburg, Russia

✉ zolotorevsky@phmf.spbstu.ru

Abstract. Slabs of low carbon bainitic steel have been subjected to various modes of fractional hot rolling at fixed conditions of the next direct quenching and tempering. To assess influence of such treatments, microstructures and textures of bainite are determined by EBSD on representative areas and then analyzed with allowance for the resulting mechanical properties. The obtained data reveal a specific effect of hot deformation as far as the tempering does not significantly change crystallographic constitution of the quenched steel. According to the bainite textures, all considered modes lead to deformed states of parent austenite; at the same time, dissimilar types of the transformation product have been detected. Specifically, the softer (granular) bainite appears at higher strains and lower temperatures of the finish rolling stage because the work hardening of austenite increases the transformation temperature. Conversely, the lath bainite providing the maximum steel strength corresponds to properly limited strains of austenite at high enough temperatures.

Keywords: bainitic steels; hot rolling; phase transformation; microstructure; strengthening

Acknowledgements. *The authors acknowledge a financial support of this work by the Russian Science Foundation, project No 22-19-00627. Microstructures were studied on the equipment of the Core shared research facilities "Composition, structure and properties of structural and functional materials" of the NRC "Kurchatov Institute" - CRISM "Prometey".*

Citation: Zisman AA, Petrov SN, Zolotorevsky NY, Yakovleva EA. Effect of industrial hot rolling mode on microstructure and properties of low carbon bainitic steel. *Materials Physics and Mechanics*. 2023;51(6): 54-64. DOI: 10.18149/MPM.5162023_5.

Introduction

Low carbon bainitic steels are widely used owing to their high strength and fracture toughness, combined with good weldability. At the same time, it is rather hard to control the properties of bainite because volume fractions of its various types depend on the plastic strain of parent austenite and the cooling rate in quenching. Moreover, the problem aggravates since such steels normally undergo the tempering that changes their properties relative to the quenched state. These issues complicate development of industrial technologies in general and become crucial in case of thick semi-products where both the strain and cooling rate are particularly non-uniform. To analyze effects of them, various combinations of hot deformation and quenching have been applied on thermo-mechanical simulators [1–3] and rolling mills [4–6]. The present paper aims to isolate specific influence of the hot rolling modes at fixed conditions of the direct quenching

and subsequent tempering. The last two operations and varied rolling parameters are relevant to industrial treatments of the considered steel.

Higher strain degrees and lower rolling temperatures, which retard both the recovery and recrystallization of austenite, generally result in increase of the transformation temperature and hence in softer bainite of granular morphology [1,2,7–9]. Conversely, the stronger lath bainite appears at lower temperatures if the parent phase undergoes weaker hardening due to less strains or/and higher rolling temperature [8,9]. However, to make use of this regularity, the quenching should be sufficiently rapid [1] as is the case in the present work. As to the tempering that diminishes the dislocation density and results in some redistribution of carbon, corresponding effects on the crystallographic constitution of bainite [10] are usually insignificant so that EBSD can reveal microstructures of the *quenched* state.

Based on EBSD orientation data, several mutually complimentary methods are employed to characterize the material state. Thus, along with the microstructure, the texture of steel can be determined. Unlike the XRD method that derives the orientation distribution function (ODF) from a number of *incomplete* pole figures, EBSD immediately expresses this function in terms of measurement results at periodically arranged discrete points. Respective complete pole figures comply with those obtained by XRD technique [11] and are often more distinct since the underlying ODF is derived from a greater set (up to 10^6) of orientations. At the same time, the opinion is spread that *representativeness* of EBSD data is inferior to that of XRD. To get proper results while avoiding a formal analysis of this issue, we employ a rather large EBSD area covering several hundreds of prior grains and the scanning step providing in each of them thousands of measurement points.

In case of bainitic or martensitic steels, which have pronounced orientation relationships (OR) between the parent and product phases, the transformation texture enables assessment of the parent austenite state because its rolling and recrystallization textures significantly differ. A simple way to recognize them [12,13] is to make use of approximate similarity between $(111)_\gamma$ and $(110)_\alpha$ pole figures. Whether reference [14–16] or measured OR are used, parallelism of these crystal planes is kept with accuracy of about one degree. At the same time, to properly distinguish between various bainite types by means of coupling statistics for admitted OR variants [17–19], a specific inter-phase relationship of any steel is needed. Following [20], each OR used in the present work is fitted to the interfacial misorientations in the final structure. Such an approach avoids errors caused by non-uniformity of deformation in prior grains and highly facilitates computations.

Apart from EBSD orientation maps, steel microstructures can be specified by respective distributions of crystal curvature (orientation gradient) that depends on the dislocation density and hence local phase constituents [10,21–23]. Among popular curvature measures [24], the grain average misorientation (GAM) is most convenient in analyzing the transformation products as far as it treats *whole* structural elements separated by closed interfaces. To properly draw the latter, their tolerance angle θ_t should correspond to the least inter-variant misorientation of the employed OR. It is worth noting that such a non-local estimate is relevant to the average density of lattice dislocations [25] rather than their “geometrically necessary” agglomerations with a net Burgers vector forming low-angle boundaries. This simplification is wittingly used in the present paper because the main contribution to strength of lath bainite or martensite is provided by the bulk dislocation density [26,27].

Materials and Methods

Chemical composition of the considered steel (wt. %: 0.08C, 0.21Si, 0.34Mn, 2.5(Ni+Cu), 0.59(Cr+Mo), 0.034V, 0.004Nb) ensures its mostly bainitic structures by quenching in a wide range of cooling rates. Three slabs of 300 mm thickness were reheated to 1200 °C and hot rolled on a reversing mill. Plates subjected to various rolling modes were directly quenched in a

sprinkler installation at the same final thickness of 18 mm and then tempered for 8.5 hours at 645 °C.

Analyzed sections normal to the transversal direction (TD) were prepared by the usual metallographic procedures and then subjected to electrolytic polishing in perchloric acid-ethanol solution at 0 °C. EBSD over areas of 2.25 mm^2 with a scanning step of 1 μm was implemented on SEM Lyra 3-XMH at an accelerating voltage of 20 kV. Crystal orientations were determined by Channel 5 software. Based on the obtained data, bainite textures have been determined by means of MTEX software and then used following [28] to reconstruct textures of parent austenite. To image morphology of bainite by the band contrast (BC), smaller areas are rescanned with a step of 0.1 μm. The related orientation data are employed to assess crystal curvature in individual laths and derive OR from inter-lath misorientations [20]. The coupling statistics for admitted variants of each specific OR is assessed on the section plane according to length fractions of respective interfaces revealed with angular accuracy of one degree.

Table 1. Hot rolling modes and respective mechanical properties of quenched and tempered steel

Rolling mode	Number of passes	Conditions of the last five passes			YS, MPa	UTS, MPa	Reduction in area, %
		Average temperature, °C	Average thickness reduction, %	Accumulated thickness reduction, %			
A	16	913	16	58	610	690	82
B	18	977	14	53	630	710	80
C	22	953	11	44	670	720	80

Table 1 lists whole numbers of rolling passes for the three applied modes and characteristics of finish rolling stages as well as resulting mechanical properties of steel (yield stress, ultimate tensile strength and reduction in area prior to fracture) determined by standard tests. First, relative thickness reductions at the last five passes are expressed by

$$\delta_i = (H_{i-1}-H_i)/H_{i-1} \quad (1)$$

at $i=N-4, N-3, \ldots, N$ where N is the whole number of passes. The table represents average values of these δ_i and of related temperatures as well as the relative thickness reduction accumulated during the last passes:

$$\Delta = (H_{N-5}-H_N)/H_{N-5}. \quad (2)$$

It is meaningful that arrangement of steel properties follows strain degrees rather than respective temperatures. As expected, less deformed austenite results in stronger bainite.

Note that the specific allowance for the finish rolling stage is motivated by two reasons. First, owing to higher temperatures of the previous passes gradually diminishing from 1200°C, the softening of austenite by its recovery or/and recrystallization in inter-pass pauses weakens influence of related deformations on the final steel properties. That is why the hot rolling mode is often specified by the least FRT (finish rolling temperature) [5,6]. In this regard, our consideration of the last five passes refines the analysis. Second, the whole complex mode is problematic to quantify by few parameters as far as averaging over too wide ranges of temperature and strain would be hardly relevant physically.

Results

Bainite microstructures and textures by EBSD. Orientation distributions at the considered rolling modes are conventionally represented in Fig. 1 by colors corresponding to TD with respect to a standard triangle of the inverse pole figure (IPF). Each of these maps demonstrates performance of EBSD on a large (2.25 mm^2) area that covers about a thousand of prior grains and presumably provides the representative texture. However, such images cannot properly

display bainite microstructures because the employed scanning step exceeds their fine scale to reasonably limit time of the data acquisition. To refine analysis as shown in inserted fragments, smaller domains have been rescanned with a step of 0.1 μm.

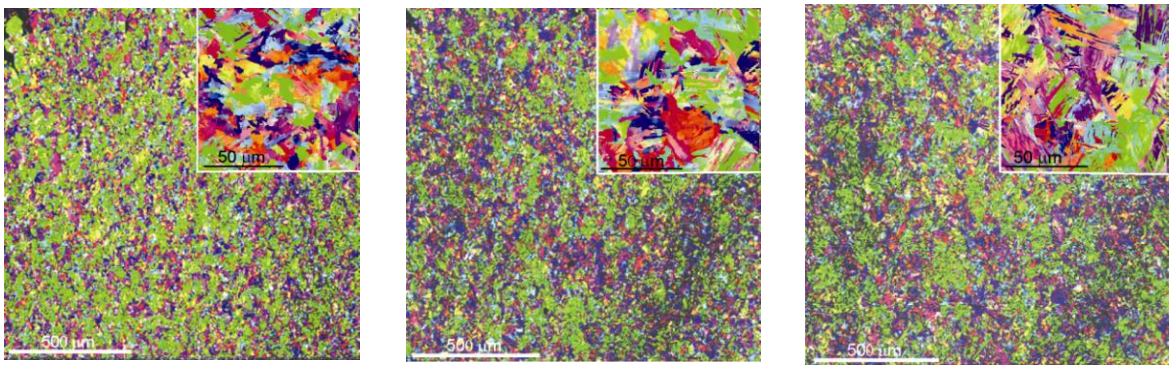

(a) (b) (c)

Fig. 1. Orientation (IPF) maps of large areas of bainite corresponding to hot rolling modes A (a), B (b) and C (c). Inserts show microstructures revealed on small areas with a finer scanning step

Figure 2 provides higher magnification of bainite microstructures by means of BC maps also derived with the refined scanning step. It is worth noting that such maps are sensitive to crystal imperfections and hence perfectly substitute metallographic images usually obtained by the chemical etching. As expected, the most pronounced lath morphology of the transformation product corresponds to the least deformed austenite (mode C) whereas the strongest work hardening of the parent phase (mode A) leads to predominance of granular bainite peculiar to higher transformation temperatures.

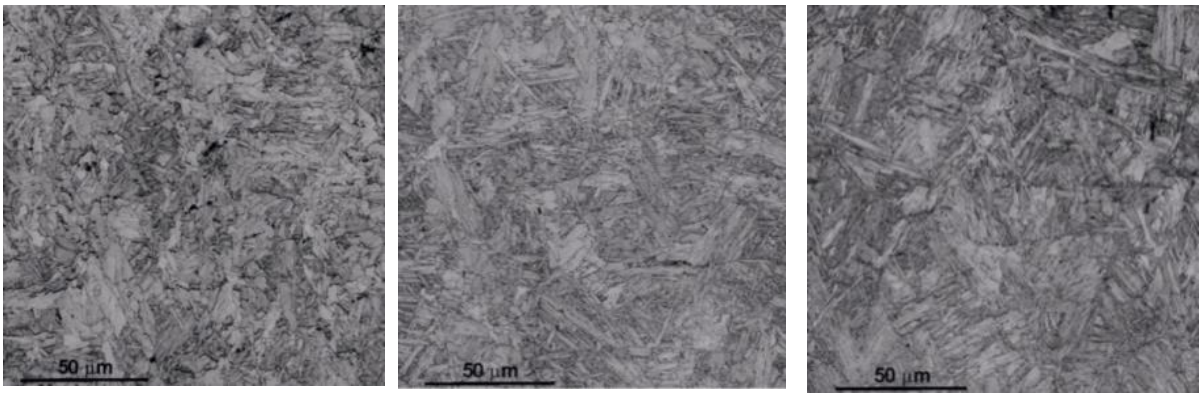

(a) (b) (c)

Fig. 2. BC maps of bainite corresponding to hot rolling modes A (a), B (b) and C (c)

Pole figures $(110)_\alpha$ of bainite close to $(111)_\gamma$ ones observed in the parent phase deformed by rolling [12] are shown in Fig. 3 where RD and TD conventionally indicate the rolling and transverse directions. Owing to the least temperatures and maximum thickness reductions, mode A results in strong components of the rolling texture which become notably weaker at modes B and C. At the same time, with respect to B, the latter texture somewhat sharpens. This effect wants explanations since it takes place at the minimum thickness reductions of austenite (Table 1) which expectedly lead to the high strength and lath morphology of the product phase. As will be discussed in the next section, the texture and hardening of austenite may not ideally correlate as far as they differently depend on deformation conditions.

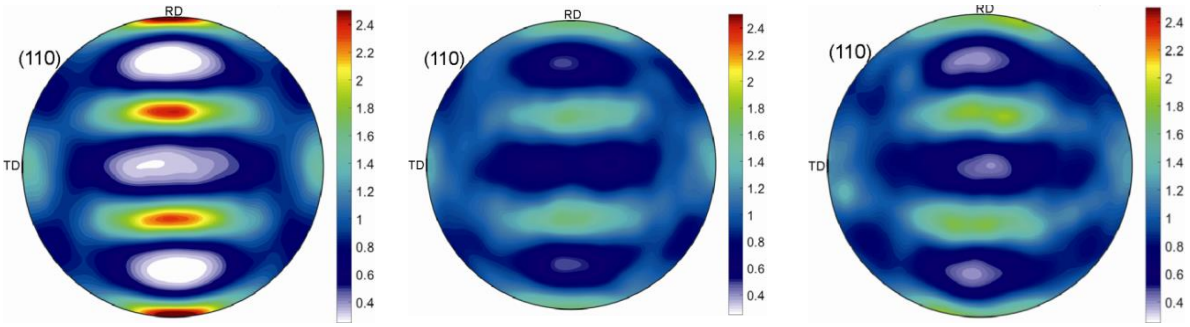

(a) (b) (c)

Fig. 3. Pole figures $(110)_\alpha$ for bainite textures corresponding to hot rolling modes A (a), B (b) and C (c)

To refine analysis, characteristic ODF sections (φ_2=45°) are represented in Fig. 4. In all, they comply with the above-considered arrangement of rolling modes in strength of related textures except for a red spot at mode B. As considered in the next subsection, such maximums of probability density, as well those at the upper right corner can appear from either parent cube component due to recrystallization of austenite or the brass component of its rolling texture. To exclude this uncertainty, the parent textures reconstructed from those of bainite will be further analyzed. With the inter-phase OR kept in mind [13], Fig. 4 evidence for predominance of the "transformed brass component" [13], though signs of the “transformed copper component” are also displayed at modes A and, somewhat weaker, at C. It should be remarked as well that at mode C several features of the transformed brass in the bainite texture differ from those of mode B.

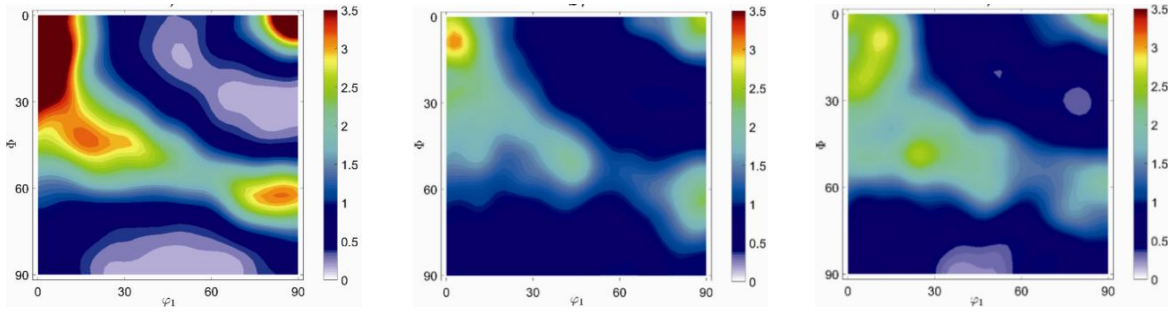

(a) (b) (c)

Fig. 4. Bainite ODF sections (φ_2=45°) corresponding to hot rolling modes A (a), B (b) and C (c)

To reveal the coupling statistics for admitted variants of whatever OR, the latter should be properly determined first. Specifically derived following [20] at the considered rolling modes, resulting OR are represented in Fig. 5(a) by the inter-phase angles between close packed planes $(111)_\gamma$ & $(110)_\alpha$ and directions $[110]_\gamma$ & $[111]_\alpha$ further called CPP and CPD, respectively. According to the last quoted work, the OR very close to that by Greninger & Troyano [15] at mode C corresponds to lath bainite whereas other two are relevant to the granular morphology of this phase.

The least inter-variant angle corresponding to each of the considered OR is about five degrees; therefore, we will carefully employ $\theta_t = 4^o$ to allow for real accuracy of measured orientations while ignoring smaller inter-lath angles within any single block (variant) of bainite. The same θ_t will be used to draw closed interfaces in determination of GAM. Coupling spectra for admitted variants of OR are shown in Fig. 5(b-d) with respect to an arbitrarily selected variant V_1 where the dashed lines indicate the average probability of considered pairs. With the

reference data [17] kept in mind, these bar charts confirm the above-mentioned microstructure types. Indeed, predominance of couples V_4/V_1 and V_8/V_1 at modes A and B evidences for granular morphology of bainite, that is, its formation at higher temperatures, whereas the strongest V_2/V_1 at mode C is characteristic of low-temperature lath bainite.

To sum up the above-considered results, the growth of steel strength with the weakened hardening of parent austenite complies with the transition from the granular to lath morphology of bainite.

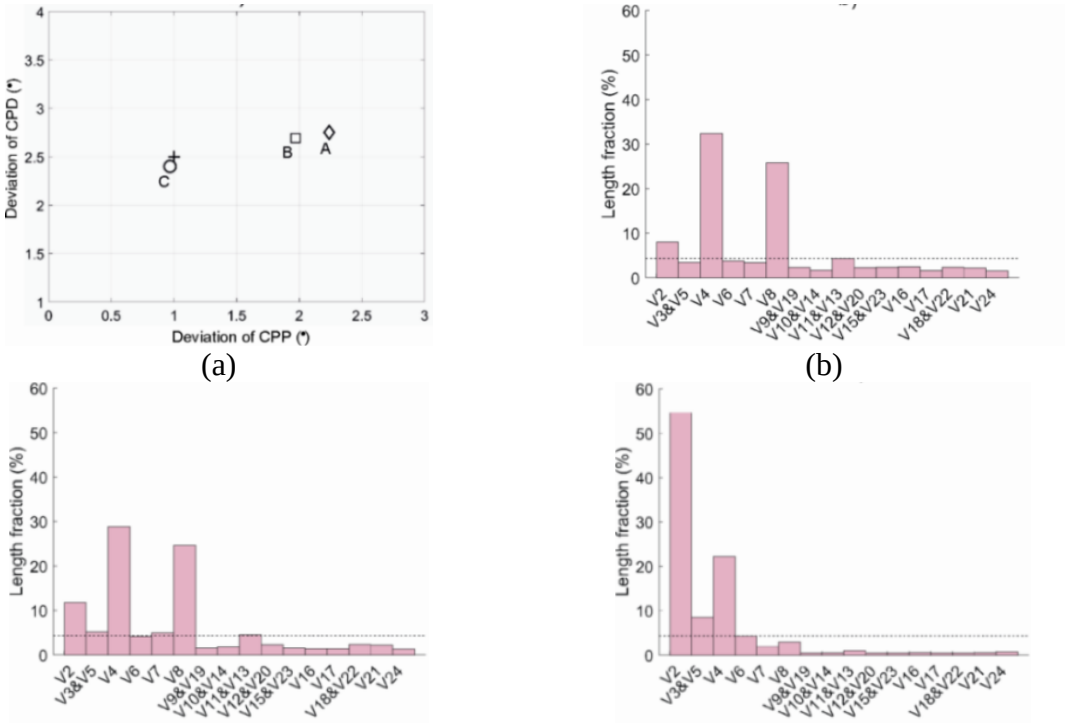

Fig. 5. (a) Inter-phase deviations of CPP and CPD for various OR corresponding to hot rolling modes A, B and C; a cross indicates the Greninger-Troyano relationship. Respective spectra in (b-d) show statistics of variant coupling with allowance for specific OR

The revealed regularity is additionally illustrated in Fig. 6 by appearance of OR variant coupling where *high-angle* V_2/V_1 boundaries expectedly predominate at mode C according to Fig. 5 and previous BC maps (Fig. 2).

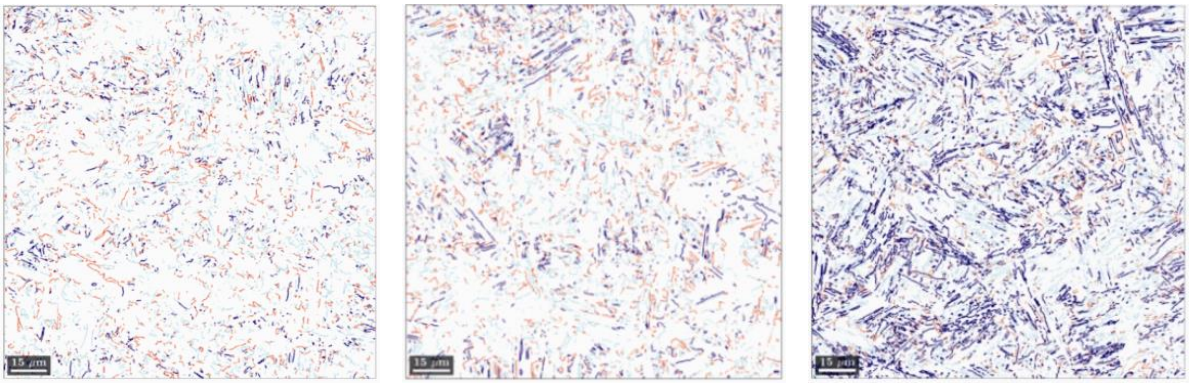

Fig. 6. Inter-variant boundaries revealed by EBSD on bainite sections at hot rolling modes A (a), B (b) and C (c). Blue, cyan and red correspond to couples V_2/V_1, V_4/V_1 and, V_8/V_1

GAM spectra of bainite corresponding to applied hot rolling modes are shown in Fig. 7(a), and the bar chart in Fig. 7(b) represents respective yield stresses and average GAM values. The two characteristics naturally prove to change in the same order. However, the former most strongly increases at mode C whereas the latter notably grows at mode B and then only slightly changes. In more detail, this difference related to the combined influence of dislocation density and morphology of bainite will be discussed after.

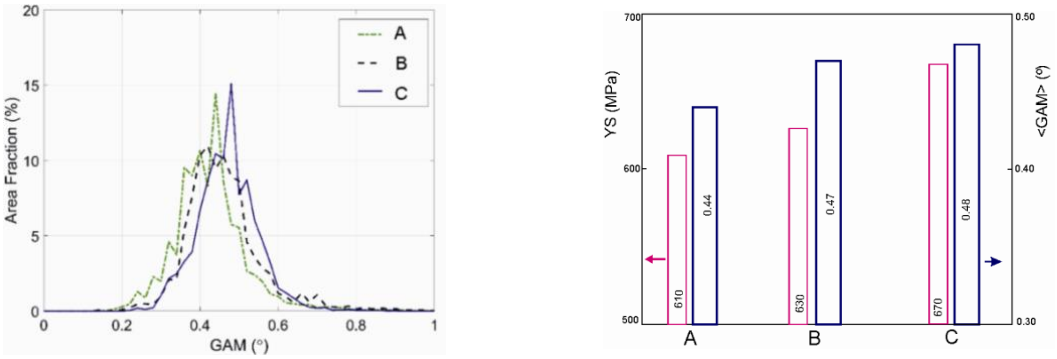

(a) (b)

Fig. 7. (a) Spectra of GAM in bainite at the three hot rolling modes;
(b) bar chart for respective yield stresses and average values of GAM

Reconstructed textures of parent austenite. Figure 8 represents pole figures $(111)_\gamma$ corresponding to the reconstructed ODF of parent austenite which satisfactorily comply with their $(110)_\alpha$ counterparts in bainite (Fig. 3) determined by EBSD. Thus, the rolling texture at mode A is very strong as compared to those of B and C, the latter of the two being somewhat sharper with respect to B.

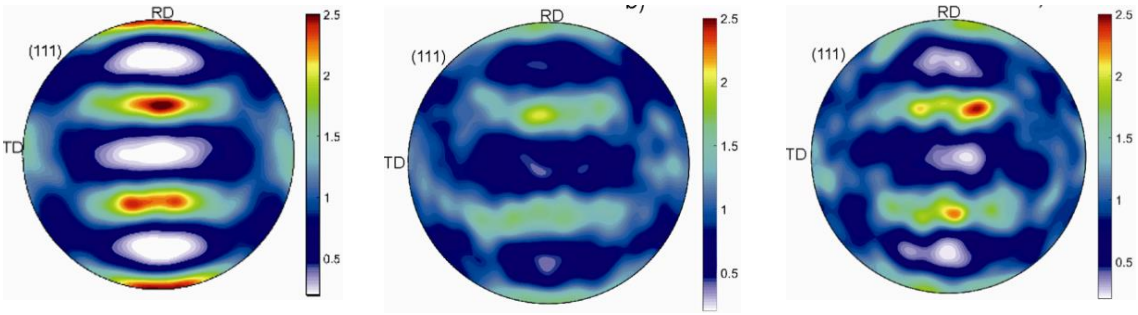

(a) (b) (c)

Fig. 8. Pole figures $(111)_\gamma$ for reconstructed textures of parent austenite corresponding to hot rolling modes A (a), B (b) and C (c)

The ODF sections for bainite (Fig. 4) are supported by respective sections for the parent phase shown in Fig. 9. They display the brass components of rolling texture (middle parts of $\Phi = 90°$ sides) at all considered modes as well as the copper components ($\varphi_1 \approx 90°$, $\Phi \approx 30°$) at modes A and, to less degree, C. Besides, positions of the ODF maximums at ($\Phi \approx 0$, $\varphi_1 \approx 45°$) in Fig. 9(a,b) reveal the cube component indicative of austenite recrystallization [13], which could *partly* transform in the maximums at upper corners of Fig. 4(a,b). However, in case of mode A this component is rather weak with respect to the pronounced brass that apparently was the main origin of such maximums. As to mode B, the *integrated* cube probability and hence the related volume fraction are still relatively small so that even in this case the two discussed features of bainite are mostly transformed from the rolling (brass) component of parent texture.

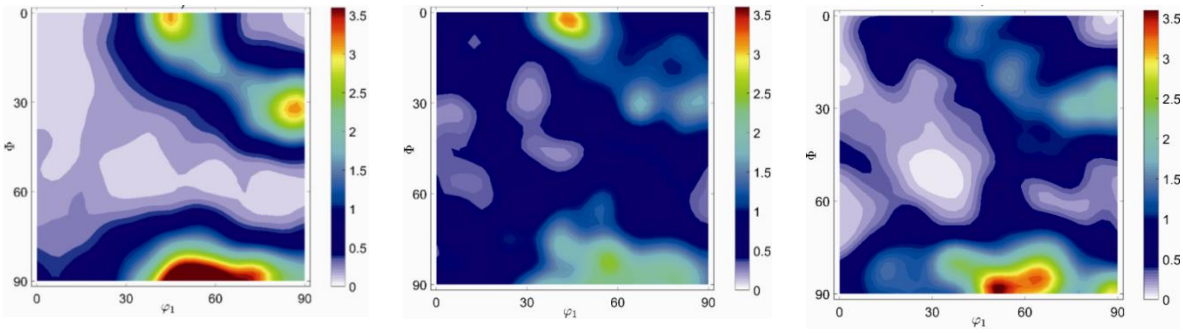

(a) (b) (c)

Fig. 9. Reconstructed ODF sections (φ_2=45°) of parent austenite corresponding to hot rolling modes A (a), B (b) and C (c)

Discussion

The present results indicate that strength of low carbon bainitic steel at various finish modes of hot rolling mostly depends on thickness reductions rather than respective temperatures. Variations of the latter *in the considered range* do not affect this regularity although somewhat influence recrystallization of parent austenite and hence its texture. In particular, with respect to mode B, the texture of bainite observed at mode C proves to be sharper and seemingly suggests stronger hardening of austenite and, as a result, softer bainite. However, the lath morphology and higher strength of the transformation product contradict to this assumption. To discuss such a paradox, we will recollect results of the previous experiments [29] on a thermo-mechanical simulator where the kinetics of *static* recrystallization in the parent phase of similar steel has been recorded at various pre-strains and temperatures. Besides, as shown in the same work, the usual conditions of fractional hot rolling exclude *dynamic* recrystallization which requires an unrealistically high thickness reduction per pass.

According to [29], at an inter-pass time lapse up to 15 s the considered stages of modes A and B admit only *incomplete* recrystallization involving a minor austenite fraction, whereas mode C completely excludes this phenomenon because of insufficient partial strains. Although Table 1 describes five rolling passes rather than a single thickness reduction employed in the above-mentioned experiments, the same regularity is supported by the reconstructed ODF sections of parent austenite. Indeed, the cube component ($\Phi\approx0$, $\varphi_1\approx45°$) appears in Fig. 9 only at modes A and B, being stronger at the latter owing to higher temperature. However, since the most part of material avoids recrystallization, the average hardening degrees in both cases should exceed that of mode C with minimum strains per pass.

Although final mechanical properties expectedly depend on strains accumulated during finish rolling stages, a question appears of why the textures corresponding to modes B and C so drastically weaken with respect to mode A (Figs. 3 and 8). This behavior may be ascribed to whether lower thickness reductions or higher temperatures as well as to their combined influence. However, to quantify the texture development in hot deformation of the *parent* phase is a very hard problem that wants special efforts beyond the scope of this work.

The reconstruction method [28] deserves a special remark as follows. Though it is mostly used to restore parent austenite structures, the corresponding textures can be also determined as demonstrated in the present work. Moreover, in the authors' opinion, this approach is generally more reliable when assessing states of the parent phase in cases, when the latter is not recrystallized. Indeed, both non-uniform deformations of prior grains and some inaccuracy of measured orientations significantly complicate the *local* structure reconstruction, whereas related random errors should be averaged out by an *overall* texture extracted from a representative EBSD scan.

Another interesting issue is the correlated growth (Fig. 7b) of average GAM and yield stress (YS) presumably dependent on dislocation density ρ according to Taylor ($\sigma \sim \rho^{1/2}$, [30]). This finding should be analyzed because the most distinct increases of the two characteristics take place at dissimilar rolling modes. One can suggest that the growth of bainite <GAM> at mode B results from the softening of parent austenite at higher temperatures, whereas the increasing YS at mode C is related to the significant lath refinement, that is, the Hall-Petch mechanism of hardening. As shown in [26], when the lath thickness diminishes to less than 1 μm, the size effect weakens and the yield stress variations can be attributed to those of dislocation density as well as solid solutions, disperse carbides and carbon atmospheres at dislocations. However, at very small fractions of carbon, as is the case for our steel, the latter three factors prove to be less significant whereas Taylor's equation becomes relevant to the main component of bainite strength. That is why it would be desirable to facilitate assessment of dislocation density in refined lath structures by making use of EBSD data as follows.

The elastic rotation field of a single dislocation is inversely proportional to distance [31] so that randomly distributed (mutually screened) dislocations with characteristic spacing L will result in the average level of crystal curvature almost linearly dependent on $\rho^{1/2} \approx 1/L$. Therefore, <GAM> should be roughly proportional to $\rho^{1/2}$, that is, the dislocation component of yield stress predominating at thin laths peculiar to lower transformation temperatures. Let alone convenience of panoramic EBSD method, it will be superior to TEM in representativeness of thus evaluated ρ and, unlike XRD, can apply to various structural scales. Of course, the corresponding estimates of dislocation density should be verified by conventional techniques [32]. Note that EBSD data are often used to quantify geometrically necessary dislocations which form low-angle boundaries and other agglomerations of Burgers vector. This is not the case in the proposed method aimed at the bulk dislocation density of any lath *as a whole*. A low tolerance angle ($\theta_t < 4^o$) for boundaries and small thickness of the laths seem to be proper reasons to ignore their inhomogeneity in the first approximation.

Conclusion

Textures and microstructures of low carbon bainitic steel have been analyzed by EBSD for various finish modes of industrial hot rolling at the same conditions of direct quenching and subsequent tempering. Although all these modes strongly decelerate or exclude recrystallization of parent austenite, the mechanical properties of steel mostly dependent on accumulated strains significantly vary. The considered data lead to the following findings:

1. To get the lath bainite providing the maximum steel strength, the thickness reduction accumulated during the finish rolling stage should be properly limited. Thus, for example, such a reduction by the last five passes of mode C did not exceed 45 %.
2. The overall texture of bainite determined on an appropriately large EBSD scan enables accurate reconstruction of the parent texture and hence assessment of austenite state prior to the steel quenching.
3. Observed at the applied hot rolling modes of low carbon steel, a correlation between its yield stresses and *average* levels of crystal curvature apparently suggests a simple way to assess the bulk dislocation density of lath bainite in terms of EBSD data.

References

1. Zhao H, Palmiere EJ. Influence of cooling rate on the grain-refining effect of austenite deformation in a HSLA steel. *Materials Characterization*. 2019;158: 109990.
2. Panpurin SN, Zolotorevsky NY, Titovets YF, Zisman AA, Khlusova EI. Crystallographic features of low-carbon bainite formed under non-isothermal conditions. *Materials Science Forum*. 2013;762: 110-115.

3. Kumar S, Manda S, Giri SK, Kundu S, Karagadde S, Balamuralikrishnan R, Murty SVSN, Anoop CR, Samajdar I. Relating martensite variant selection with prior austenite microstructure: A coupled study of experiments and pixel-by-pixel reconstruction. *Materials Characterization*. 2023;199: 112822.
4. Kaijalainen A, Javaheri V, Lindell D, Porter DA. Development of crystallographic texture under plane and shear strain in ultrahigh-strength strip steels. *Materials Science and Engineering A.* 2018;375: 012026.
5. Bernier N, Bracke L, Malet L, Godet S. Crystallographic reconstruction study of the effects of finish rolling temperature on the variant selection during bainite transformation in C-Mn high-strength steels. *Metallurgic and Materials Transactions A*. 2014;45: 5937–5955.
6. Wang H, Chen Y. The effect of finish rolling temperature on the microstructure and properties of non-quenched and tempered bainite steel. *Procedia Engineering*. 2017;207: 1839–1843.
7. Cizek P, Wynne BP, Davies CHJ, Muddle BC, Hodgson PD. Effect of composition and austenite deformation on the transformation characteristics of low-carbon and ultralow-carbon microalloyed steels. *Metallurgic and Materials Transactions A*. 2002;33: 1331–1349.
8. Lan L, Yu M, Qiu C. On the local mechanical properties of isothermally transformed bainite in low carbon steel. *Materials Science and Engineering A.* 2019;742: 442–450.
9. De-Castro D, Eres-Castellanos A, Vivas J, Caballero FG, San-Martín D, Capdevila C. Morphological and crystallographic features of granular and lath-like bainite in a low carbon microalloyed steel. *Materials Characterization*. 2022;184: 111703.
10. Zisman AA, Zolotorevsky NYu, Petrov SN, Khlusova EI, Yashina EA. Panoramic crystallographic analysis of structure evolution in low-carbon martensitic steel under tempering. *Metal Science and Heat Treatment*. 2018;60: 142–149.
11. Eres-Castellanos A, Morales-Rivas L, Jimenez JA, Caballero FG, Garsia-Mateo C. Effect of ausforming on the macro- and micro-texture of bainitic microstructures. *Metallurgic and Materials Transactions A.* 2021;52: 4033.
12. Brown EL, Deardo AJ. On the origin of equiaxed austenite grains that result from the hot rolling of steel. *Metallurgic and Materials Transactions A*. 1981;12: 39–47.
13. Jonas JJ. Transformation textures associated with steel processing. In: Haldar A, Suwas S, Bhattacharjee D. (eds.) *Microstructure and Texture in Steels*. New York: Springer; 2009; p.3–17.
14. Kurdjumov G, Sachs Z. Uber den machanismus der stahlhartung. *Zeitschrift für Physic*. 1930; 64: 325–343.
15. Greninger AB, Troyano AR. The mechanism of martensite formation. *Metals Transactions*. 1949; 185: 590–598.
16. Nishiyama Z. Lattice distortion and atomic displacements during the fcc/bcc martensitic transformation. *Scientific Reports of the Tohoku Imperial University*. 1932;3: 637–644.
17. Miyamoto G, Iwata N, Takayama N, Furuhara T. Quantitative analysis of variant selection in ausformed lath martensite. *Acta Materialia*. 2012;60(3): 1139–1148.
18. Takayama N, Miyamoto G, Furuhara T. Effects of transformation temperature on variant pairing of bainitic ferrite in low carbon steel. *Acta Materialia*. 2012;60(5): 2387–2396.
19. Stormvinter A, Miyamoto G, Furuhara T, Hedström P, Borgenstam A. Effect of carbon content on variant pairing of martensite in Fe–C alloys. *Acta Materialia.* 2012;60(20): 7265–7274.
20. Zolotorevsky NY, Panpurin SN, Zisman AA, Petrov S.N. Effect of ausforming and cooling condition on the orientation relationship in martensite and bainite of low carbon steels. *Materials Characterization*. 2015;107: 278–282.
21. Adams BL, Wright SI, Kunze K. Orientation imaging: The emergence of a new microscopy. *Metallurgic and. Materials Transactions A.* 1993;24: 819–831.
22. Tomaz RF, Santos DB, Camey K, Barbosa R, Andrade MS, Escobar DP. Complex phase quantification methodology using electron backscatter diffraction (EBSD) on low manganese

high temperature processed (HTP) microalloyed steel. *Journal of Materials Research and Technology*. 2022;8(2): 2423–2431.
23. Breumier S, Ostormujof TM, Frincu B, Gey N, Couturier A, Loukachenko N, Aba-perea PE, Germain L. Leveraging EBSD data by deep learning for bainite, ferrite and martensite segmentation. *Materials Characterization*. 2022;186: 111805.
24. Wright S, Nowell M, Field D. A review of strain analysis using electron backscatter diffraction. *Microscopy and Microanalysis*. 2011;17: 316–329.
25. Zisman AA, Zolotorevsky NY, Petrov SN, Ermakova NY. Effect of cooling rate on the bainite fraction in low carbon martensitic steel: combined analysis of transformation kinetics and crystal curvature. *Letters on Materials.* 2023;13: 67–72.
26. He SH, He BB, Zhu KY, Huang MX. On the correlation among dislocation density, lath thickness and yield stress of bainite. *Acta Materialia*. 2017;135: 382–389.
27. Kennett SC, Krauss G, Findley KO. Prior austenite grain size and tempering effects on the dislocation density of low-C Nb–Ti microalloyed lath martensite. *Scripta Materialia*. 2015;107: 123–126.
28. Niessen F, Nyyssonen T, Gazder AA, Hielscher R. Parent grain reconstruction from partially or fully transformed microstructures in MTEX. *Journal of Applied Crystallograhy*. 2022;55: 180–194.
29. Knyazyuk TV, Novoskoltsev NS, Zisman AA, Khlusova EI. Influence of niobium microalloying on the kinetics of static and dynamic recrystallization during hot rolling of medium-carbon high-strength steels. *Inorganic Materials: Applied Research*. 2020;11: 1325–1332.
30. Taylor GI. The mechanism of plastic deformation of crystals. Part I. *Proceedings of the. Royal Society of London*. 1934;145: 362–387.
31. de Wit R. Theory of disclinations: IV. Straight dislocations. *Journal of Research of the National Bureau of Standards*. 1973;77A: 607–658.
32. Gallet J, Perez M, Guillou R, Ernoud C, Le Bourlot C, Langlois C, Beausir B, Bouzy E, Chaise T, Cazottes S. Experimental measurement of dislocation density in metallic materials: A quantitative comparison between measurements techniques (XRD, ECCI, HR-EBSD, TEM). *Materials Characterization*. 2023;199: 112842.

THE AUTHORS

Zisman A.A.
e-mail: crism_ru@yahoo.co.uk

Petrov S.N.
e-mail: petrov.epma@mail.ru

Zolotorevsky N.Yu.
e-mail: zolotorevsky@phmf.spbstu.ru

Yakovleva E.A.
e-mail: mail@crism.ru